NAVAL POSTGRADUATE SCHOOL
Monterey, California

THESIS

THE ROLE OF VISCOUS FINGERING IN THE SEPARATION MECHANICS OF THIN INTERFACIAL LIQUID LAYERS

by

Christopher H. Rehkop

March 2000

Thesis Advisor: Ashok Gopinath

REPORT DOCUMENTATION PAGE

Form Approved OMB No. 0704-0188

1. AGENCY USE ONLY *(Leave blank)*	2. REPORT DATE	3. REPORT TYPE AND DATES COVERED
	March 2000	Master's Thesis

4. TITLE AND SUBTITLE:
The Role of Viscous Fingering in the Separation Mechanics of Thin Interfacial Liquid Layers

5. FUNDING NUMBERS

6. AUTHOR(S)
Rehkop, Christopher H.

7. PERFORMING ORGANIZATION NAME(S) AND ADDRESS(ES)
Naval Postgraduate School
Monterey CA 93943-5000

8. PERFORMING ORGANIZATION REPORT NUMBER

9. SPONSORING/MONITORING AGENCY NAME(S) AND ADDRESS(ES)

10. SPONSORING/MONITORING AGENCY REPORT NUMBER

11. SUPPLEMENTARY NOTES
The views expressed here are those of the authors and do not reflect the official policy or position of the Department of Defense or the U.S. Government.

12a. DISTRIBUTION/AVAILABILITY STATEMENT
Approved for public release; distribution is unlimited.

12b. DISTRIBUTION CODE

13. ABSTRACT ***(maximum 200 words)***

The mechanics of separation of a thin interfacial liquid layer trapped between two parallel surfaces was studied in a controlled manner. Different liquid viscosities, layer thicknesses and separation velocities were used to investigate the extensional behavior and determine its dependence on viscous fingering, and Capillary number. Force, displacement and time data have been recorded for all experimental runs. Qualitative visual data have also been recorded to corroborate the trends in the onset of viscous fingering based on a simple interfacial stability analysis. The quantitative data has been used to generate force-displacement plots of the separation. The results of this work provide useful fundamental insight into the mechanics of this novel problem.

14. SUBJECT TERMS
Thin Interfacial Liquid Layers, Capillary Number, Surface Tension, Viscous Fingering, Saffman Instability, Hele-Shaw Flow, Creeping Flows

15. NUMBER OF PAGES 64

16. PRICE CODE

17. SECURITY CLASSIFICATION OF REPORT	18. SECURITY CLASSIFICATION OF THIS PAGE	19. SECURITY CLASSIFICATION OF ABSTRACT	20. LIMITATION OF ABSTRACT
Unclassified	Unclassified	Unclassified	UL

NSN 7540-01-280-5500

Standard Form 298 (Rev. 2-89)
Prescribed by ANSI Std. 239-18 298-102

Approved for public release; distribution is unlimited

THE ROLE OF VISCOUS FINGERING IN THE SEPARATION MECHANICS OF THIN INTERFACIAL LIQUID LAYERS

Christopher H. Rehkop
Lieutenant, United States Navy, CEC
B.S., The Pennsylvania State University, 1993

Submitted in partial fulfillment of the
requirements for the degree of

MASTER OF SCIENCE IN MECHANICAL ENGINEERING

from the

NAVAL POSTGRADUATE SCHOOL
March 2000

ABSTRACT

The mechanics of separation of a thin interfacial liquid layer trapped between two parallel surfaces was studied in a controlled manner. Different liquid viscosities, layer thicknesses and separation velocities were used to investigate the extensional behavior and determine its dependence on viscous fingering, and Capillary number. Force, displacement and time data have been recorded for all experimental runs. Qualitative visual data have also been recorded to corroborate the trends in the onset of viscous fingering based on a simple interfacial stability analysis. The quantitative data has been used to generate force-displacement plots of the separation. The results of this work provide useful fundamental insight into the mechanics of this novel problem.

TABLE OF CONTENTS

LIST OF FIGURES

ACKNOWLEDGMENTS

I would like to express my great appreciation to Professor Ashok Gopinath for his support throughout this research. His dedicated guidance has significantly enhanced my education at the Naval Postgraduate School. I also would like to thank my wife for her understanding and inspiration.

I. INTRODUCTION

The original studies on the instability of the interface between two liquids were carried out in the late 1950s, when water was pumped down into an apparently 'dry' oil field to push up the remaining oil. The belief was that the oil being lighter than water would rise, although in reality the interface between the water and oil was unstable and fingers of water penetrated up through the ground leaving the oil down below. It was shown by Taylor (1958), and Saffman and Taylor (1958), in a now classic study that the phenomenon could be explained by a simple analysis based on Darcy's law for flow of a viscous fluid through a homogeneous porous medium.

The study of the motion of fingers of a less viscous fluid through a more viscous fluid in a Hele-Shaw cell (i.e. in a narrow gap between parallel plates.) is a paradigm in applied mathematics. It has raised questions at all levels. By choosing the proper equations of motion, it can be solved analytically or numerically. Considerable experimental evidence has also been gathered for various scenarios. Continuing disagreement with experiments leads to modifications of the assumptions and approximations employed by the theory until good agreement is reached to help understand the phenomenon (Saffman, 1991).

It has been shown that for a channel of given aspect ratio (width/thickness of the layer), it was found for the case when the viscosity of the displacing fluid is negligible that the shape and width of the fingers depend only on the Capillary number (Ca). A way to measure the ratio of viscous forces to surface tension is through the use of the Capillary number ($Ca = \mu U/\sigma$). If the capillary number remains small (10^{-2}–10^{-6}), the surface tension effects are expected to dominate the flow. The combination of the liquid

viscosity and interface velocity could be chosen in such a way that the capillary number would be in the above limits. Also, by keeping the aspect ratio large ($D/l_0 >> 1$), the fluid mechanics in the layer could be restricted to essentially one-dimensional behavior.

In this experiment, the approach to the problem is different. A tensile force is applied to a layer of liquid trapped between two circular parallel disks and the force-displacement behavior is studied vis-a-vis the onset of viscous fingering. A wide range of viscosities, separation velocities and initial liquid layer thicknesses are explored.

A variation of the Saffman-Taylor instability analysis will be used to determine the neutral stability curve and the most dangerous wavelength that grows into fingers, as well as the number of corrugations (fingers) that form. Through experimental analysis of the data, the interface velocity and the Capillary number at the point of viscous fingering can be calculated with extreme accuracy and repetition.

Quantitative force-displacement data and qualitative visual data have been gathered for this experimental study. Both forms of data have been used to make some useful deductions of the mechanics of separation of thin interfacial liquid layers.

II. BACKGROUND

A. SURFACE TENSION

1. Theoretical Background

The effects of surface and interfacial tensions give rise to so many phenomena observed in liquid behavior that the complex physical-chemical interactions involved are taken for granted and not all of which are understood even today. The liquid state itself is composed of molecules in motion that are kept relatively close to each other by attractive Van der Waals forces. However, a principal method of analysis of problems of interfacial effects rests upon the assumption that a *mean molecular field* can describe the liquid. It is assumed possible to define an element of the liquid that is small compared to the range of intermolecular forces but large enough to contain a sufficient number of molecules. This approximation implies that on average the attractive force on any molecule in the liquid is the same in all directions giving to the liquid its fluid characteristics (Probstein, 1989).

2. Liquid-Gas Interface

At a liquid-gas interface although the molecules are free to move in the liquid, their motion is far more restricted than in a gas where there is a little attraction between the molecules. Therefore the attraction between the liquid molecules will prevail and prevent the liquid molecules from escaping into the gas. As a result, the liquid molecules at the surface are attracted inward and normal to the liquid-gas interface, which us equivalent to the tendency of the surface to contract.

If the interface is curved, a mechanical balance shows that there is a pressure difference across the interface. The pressure is higher on the concave side. Two surface

tension forces balance the pressure increase in the interior. For an arbitrary curved interface whose principal radii of curvature are R_1 and R_2 and have a surface tension σ. A force balance normal to the surface will show that the pressure differential is

$$\Delta p = \sigma\left(\frac{1}{R_1} + \frac{1}{R_2}\right) \tag{1}$$

The previous equation is known as the Young-Laplace Equation. For a special case of a spherical bubble or drop in immiscible liquids, a well-known result is obtained, where r is the bubble or drop radius.

$$\Delta p = \frac{2\sigma}{r} \tag{2}$$

When a drop is placed on a plane solid surface, it will be in contact not only with the surface but also with a gas such as air. The liquid may spread freely over the surface, or it may remain as a drop with a specific angle of contact with the solid surface. A force balance would involve both surface tension (σ) and contact angle (θ). If the contact angle is less than 90°, the liquid is said to *wet* the solid; if the contact angle is greater than 90°, the liquid is *nonwetting* (White, 1994).

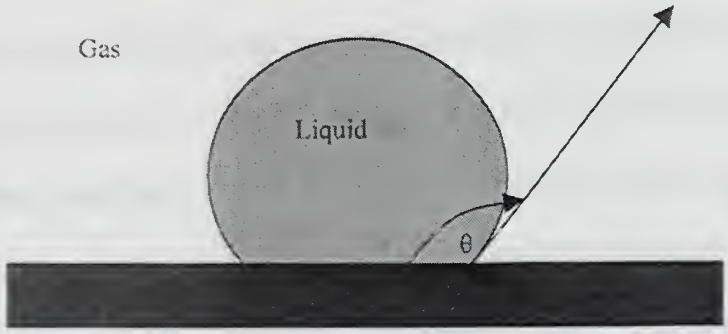

Figure 1. Static Contact Angle Between Liquid and Gas Interface.

3. Capillary Number (Ca)

A dimensionless quantity which plays a significant role in determining the effect at the interface of the liquid-gas boundary is the capillary number (Ca). The capillary number measures the ratio of the viscous force to surface tension force and is defined by A small capillary number indicates that the viscous forces are not dominating the flow,

$$Ca = \frac{\text{viscous force}}{\text{surface tension force}} = \frac{\mu U}{\sigma} \tag{3}$$

the surface tension acts as a stabilizing factor in examining the effects of viscous fingering.

B. VISCOUS FINGERING

1. Theoretical Background

An important instability phenomenon that has a widespread importance in this experiment is viscous fingering. This is essentially an instability of bounded creeping flows, such as appear in a porous medium or a Hele-Shaw cell, when one fluid is displaced by a second fluid of lower viscosity. Differential pressures imposed at the open boundaries could be the driving mechanism for the flow. The fundamentals of creeping flows and Hele-Shaw flows are first briefly reviewed before applying them to the viscous fingering relevant to this study.

2. Creeping Flows

Some approximate solutions of the Navier-Stokes equations for a limited case when the viscous forces are considerably greater than the inertia forces can be made. Since the inertia forces are proportional to the square of the velocity whereas the viscous

forces are only proportional to its first power, it is easy to appreciate mathematically a flow for which viscous forces are dominant. Under these conditions the Reynolds number is very small and the inertia terms can be simply omitted from the equations of motion as a first order approximation. It can be seen that the incompressible form of the Navier-Stokes equations given by

$$\rho \frac{D\mathbf{w}}{Dt} = -\,grad\, p + \mu \nabla^2 \mathbf{w} \tag{4}$$

with the inertia terms neglected become

$$grad\, p = \mu \nabla^2 \mathbf{w} \tag{5}$$

The same boundary conditions as the full Navier-Stokes equations must be introduced to the system of equations, namely those expressing the absence of fluid slip at the walls.

3. Hele-Shaw Flows

A solution of the three-dimensional equations of creeping motion can be obtained for the case of flow between two parallel flat walls separated by a small distance 2h. If a cylindrical body of arbitrary cross-section is inserted between the two plates at right angles so that it completely fills the space between them, the resulting streamlines is identical with that in potential flows about the same shape. It can be shown that the solution for creeping motion then possesses the same streamlines as the corresponding potential flow (Schlichting, 1979).

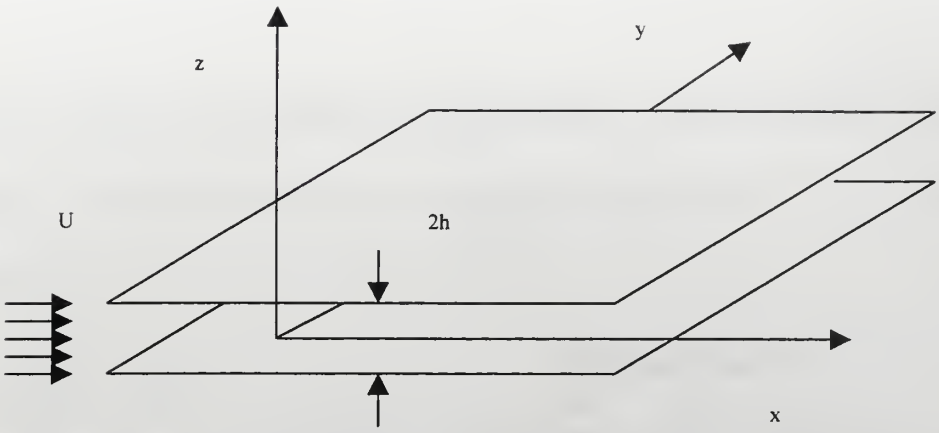

Figure 2. Hele-Shaw Cell.

We select a system of coordinates with its origin in the center between the two plates, and make the x, y-plane parallel to the plates, the z-axis being perpendicular to them as in Figure 2. The body is assumed to be placed in a stream of velocity U, parallel to the x-axis.

From the continuity equation, assuming two-dimensional, incompressible, fully developed flow

$$\frac{\partial u}{\partial x} = 0 \qquad \frac{\partial w}{\partial z} = 0 \tag{6}$$

In addition, the x-momentum equation simplifies to

$$\frac{\partial P}{\partial x} = \mu \frac{\partial^2 u}{\partial z^2} \tag{7}$$

Integrating with respect to z and applying the boundary conditions, $\partial u/\partial z = 0$ @ $z = 0$ and $u = 0$ @ $z = \pm h/2$ leads to a velocity profile

$$u = \frac{1}{\mu}\frac{\partial P}{\partial x}\frac{1}{2}\left(z^2 - \frac{h^2}{4}\right) \tag{8}$$

From the velocity profile the average velocity is obtained

$$\overline{U} = -\frac{h^2}{12\mu}\frac{\partial P}{\partial x} \tag{9}$$

4. Viscous Fingering

The Saffman–Taylor instability at an interface could arise when two fluids of different viscosity are pushed by a pressure gradient through a Hele-Shaw cell. The instability is in many ways similar to the Rayleigh-Taylor instability; the primary difference is that the equilibrium state in the former is a dynamic one, in which the interface between the two fluids is moving rather than stationary (Faber, 1997).

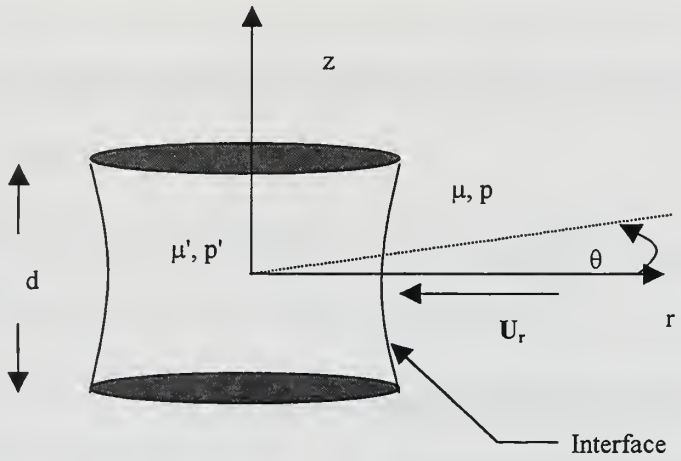

Figure 3. Side View of Radial Hele-Shaw Cell.

Here we closely follow and adapt the development by Faber (1997). Suppose the cell is horizontal, consisting of two parallel radial disks, gravitational effects can be ignored. There is a pressure gradient, which drives the fluid in the radial (+r) direction with some uniform velocity (U_r). At equilibrium, the interface between the two fluids is a concentric circle $R = U_r t$. Where $r < U_r t$, the fluid viscosity is denoted by μ'; where r

>U_r t, the viscosity is given by μ. Using the Navier-Stokes equations in cylindrical coordinates, the pressure gradient needed to maintain this motion of the two fluid regions are given by

$$\frac{\partial p'}{\partial r} = -\frac{12\mu' U_r}{d^2} \qquad \frac{\partial p}{\partial r} = -\frac{12\mu U_r}{d^2} \tag{10}$$

Where U_r is the average interface velocity and d is the disk separation distance. The pressures p′ and p are not necessarily equal at the interface, because the interface may be curved in the z direction.

$$p = -\frac{12\mu U_r}{d^2}\left(r - U_r t\right) + p_o \qquad p' = -\frac{12\mu' U_r}{d^2}\left(r - U_r t\right) + p_o \tag{11}$$

Now suppose that the interface is perturbed in a way that at time t the nominally circular interface lies at r = R, where

$$R = U_r t + \zeta_k e^{ikr\theta} \tag{12}$$

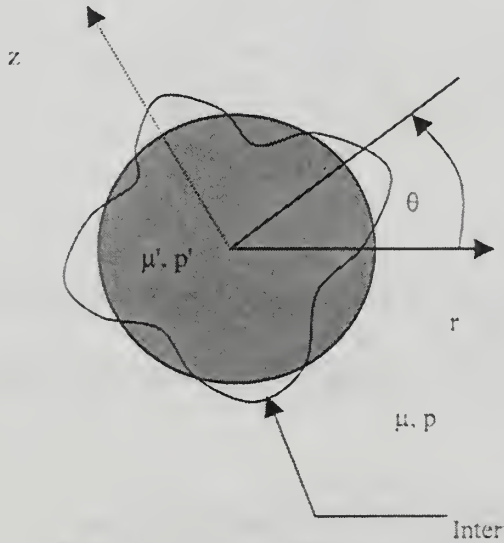

Figure 4. Plan View of Radial Hele-Shaw Cell.

There must be some corresponding perturbation in p′ and p, and it must have the same periodicity in the r direction. Any perturbation can be expressed as an infinite sum of wavelike functions. Since the perturbation cannot effect the pressure at large distances, these pressure terms have the form

$$p = -\frac{12\mu U_r}{d^2}\left(r - U_r t\right) + p_o + Ce^{k(r-U_r t)}$$

$$p' = -\frac{12\mu' U_r}{d^2}\left(r - U_r t\right) + p_o + C'e^{k(r-U_r t)} \tag{13}$$

where $k = 2\pi/\lambda$, and C′ and C are constants to be determined by boundary conditions at the interface. The boundary conditions, applicable in each case at r = R, and linearized by omission of the higher order terms yield

$$U_r' = U_r = \frac{\partial R}{\partial t} \tag{14}$$

$$-\frac{d^2}{12\mu'}\frac{\partial p'}{\partial r} = -\frac{d^2}{12\mu}\frac{\partial p}{\partial r} = U_r + \frac{\partial \zeta}{\partial t}e^{ikr\theta} \tag{15}$$

which corresponds to

$$-\frac{d^2 k}{12\mu'}C' = -\frac{d^2 k}{12\mu}C = \frac{\partial \zeta}{\partial t}e^{ikr\theta} \tag{16}$$

The pressure differential due to the interfacial surface tension is

$$p' - p = -\sigma\frac{\partial^2 R}{\partial r^2} = \sigma k^2\theta^2\zeta_k e^{ikr\theta} \tag{17}$$

The corresponding growth rate s_k can be found to be

$$s_k = \frac{1}{\zeta_k}\frac{\partial \zeta_k}{\partial t} = \frac{1}{\mu + \mu'}\left\{\frac{\sigma k^3 d^2}{12} - U_r k(\mu - \mu')\right\} \tag{18}$$

It may be noted that the interface is stable for all values of k when $\mu' < \mu$. When $\mu < \mu'$, i.e. a viscous fluid is being displaced by a less viscous one, the interface can become unstable. The neutral stability curve corresponding to zero growth rate shows that it is marginally stable for the critical wavenumber $k = k_c$ where

$$k_c^2 = \frac{12U_r(\mu' - \mu)}{\sigma d^2} \tag{19}$$

So for wavelengths $\infty > \lambda > \lambda_c$ the interface is unstable. The perturbation that grows the fastest is when s_k is a maximum, which yields the most dangerous wavelength as

(20)

$$k_{max} = \frac{k_c}{\sqrt{3}} \quad \text{or}$$

$$\lambda_{max} = \lambda_c \sqrt{3} \tag{21}$$

This corresponds to a wavelength (λ_{max}) which is the fastest growing disturbance and hence the one most likely to develop into fingers

$$\lambda_{max} = \pi d \sqrt{\frac{\sigma}{U(\mu' - \mu)}} \tag{22}$$

The largest value of the wavelength, which is consistent with the circular geometry of the flow cell of radius, r, is

$$\lambda_{largest} = 2\pi r \tag{23}$$

Then for a given combination of interface velocity, gap separation, surface tension and fluid viscosities, the most dangerous wavelength can be found and the number of fingers that consequently appear can be calculated from

$$N = \frac{2\pi r}{\lambda_{\max}} \tag{24}$$

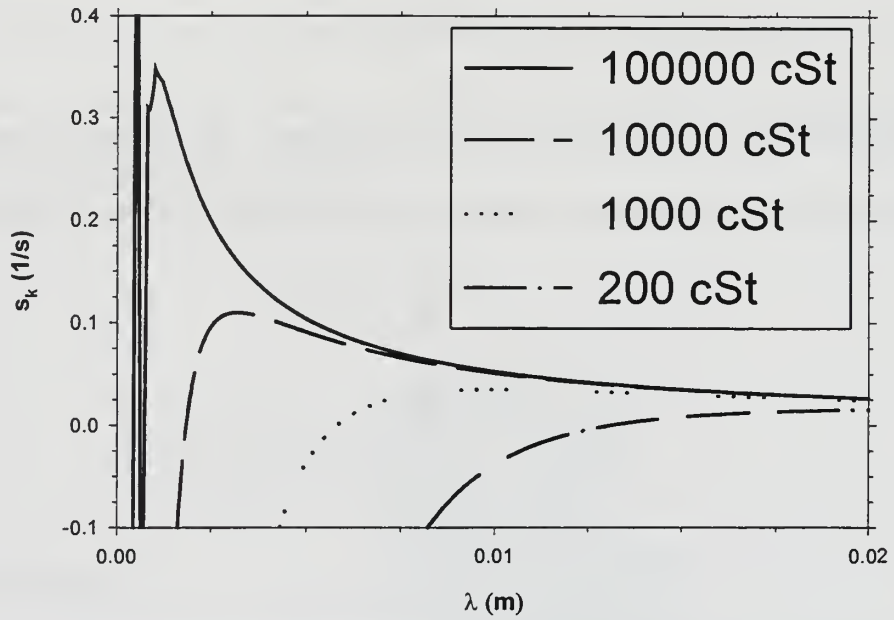

Figure 5. Growth Rate vs Wavelength (Radial velocity and Displacement Constant).

Figure 5 is a typical plot of the growth rate as a function of wavelength for a given separation velocity. The plot clearly shows that the viscosity of the fluid affects growth rate and its magnitude increases with increasing viscosity. It can also be said that the maximum growth rate is not only larger, but the peak is also more pronounced, for higher viscosities.

C. PREVIOUS STUDIES

The paper by Paterson (1981) is the only earlier study to have dealt with radially driven flow in a circular Hele-Shaw cell. An approximate equation for the growth of viscous fingers was proposed. To model the initial growth of fingers, Darcy's Law for governing the velocity of flow in a porous medium or Hele-Shaw was used. An equation for critical wavelength was obtained, and it was shown that if the circumference of the injected bubble was less than the critical wavelength the interface was stable and no viscous fingering was present. In the review by Saffman (1991) the selection mechanism and stability of fingers and bubbles in the Hele-Shaw Cells were discussed. The main focus was to better understand the uncertainties with respect to anomalously thin fingers and the nature of the finite amplitude of the instabilities. He suggested that the uncertainty in the boundary conditions at the moving interface may be the cause for the difference in the theoretical and experimental results. It was also noted that for unsteady fingering the problem is not yet resolved and many open questions remain especially since unsteady flows form singularities in finite time.

In a recent experimental study by Maxworthy (1989), the study of the stability of the circular interface in a Hele-Shaw when air displaces a viscous oil has been used to estimate the critical wavelength for large capillary numbers (Ca). A number of questions have arisen about determining the exact boundary conditions to be applied at the interface, which was slightly modified in this experimental study. The experimental results had a tendency to approach a wavelength that is a constant multiple of the gap width for values of Ca greater than unity. The reasons for this discrepancy are due to the non-zero finite nature of the Reynolds number, and three-dimensional effects.

THIS PAGE INTENTIONALLY LEFT BLANK

III. OBJECTIVES OF THE PRESENT STUDY

The objective of the present study is to obtain some fundamental insight into the onset of viscous fingering subjected to tensile forces. Unlike previous studies in this field, the main focus is the mechanics of separation of a thin liquid layer trapped between two parallel surfaces, which are being pulled apart at a constant velocity normal to the liquid layer. There is no shear or compressive forces acting on the sample. A mathematical equation is derived assuming a Hele-Shaw relationship for the onset of viscous fingering, known as the critical wavelength. A similar relationship will also be developed for the maximum growth rate of the viscous fingers, known as the maximum wavelength, which will then determine the number of fingers produced. The velocity of the interface and separation of the disks will be investigated. Experiments have been conducted and will be correlated to the mathematical equation to the onset and maximum growth of the viscous fingers. The work is experimental in nature and is aimed to gather both qualitative and quantitative data. Experiments have been planned and conducted in a way that some fundamental insights about the effects of critical wavelength interface velocity, separation distance and fluid viscosity. This study also aims to analyze the different competing regimes in the fluid deformation process.

THIS PAGE INTENTIONALLY LEFT BLANK

IV. EXPERIMENT

A. SELECTION OF THE MODEL SYSTEM

Since this experimental study involves a liquid layer in tension (normal to the plane of the layer), the experimental apparatus was constructed to apply a purely tensile force in the vertical direction. The initial separation of the plexi-glass disks in which the liquid layer resides is about 100 μm. The stage that contained the plexi-glass disks was constructed to ensure that the mating surfaces of the disks were parallel to one another. The plexi-glass disks were also developed to ensure parallelism of their mating own surfaces. The vertical travel of the positioning actuator was aligned to prevent any shear force to develop during the experimental procedure. The alignment of the vertical actuator and plexi-glass disks were perfectly perpendicular to the direction of the separation movement. Figure 6 shows the experimental apparatus, the supporting structure was constructed of high grade aluminum and mounted on a permanent rigid support platform to prevent any deviation from the normal.

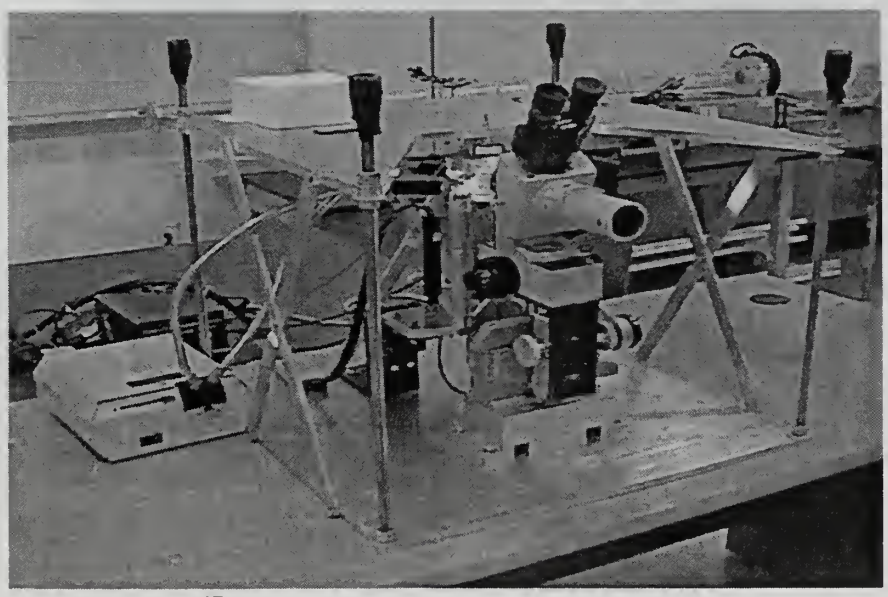

Figure 6. Experimental Set-Up, Apparatus.

The experimental set-up was designed to gather both numerical and visual data. One CCD camera was placed in the set-up to provide this required data. Since one of the objectives of the experiment was to determine onset of viscous fingering, the CCD camera was positioned to record the movements of the liquid layer from the bottom of the plexi-glass disks. This camera was mounted on the vertical moving stage (to move together with the disks) to prevent the focal length from changing during the operation of the experiment (Figure 7). The CCD camera was connected to monitors for viewing and recording.

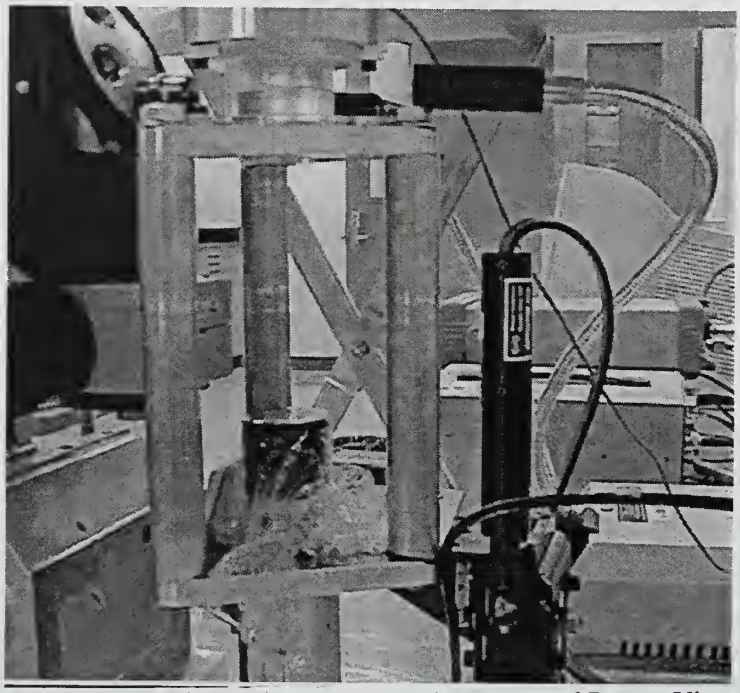

Figure 7. Movable Stage, Plexi-glass disks, Actuator, Microscope and Bottom View CCD Camera.

Figure 8. Experimental set-up, Computer, 855C Programmable Controller, Multimeter, Amplifier.

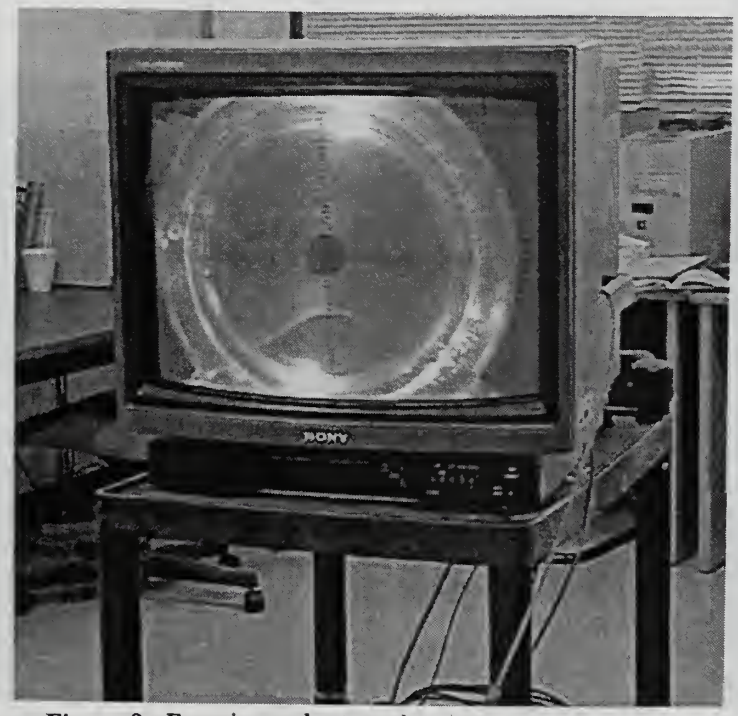

Figure 9. Experimental set-up showing monitor for bottom view.

The computer was used to run and store data for latter use and analysis (Figure 8). A software program written for this particular experiment controlled the vertical movement of the actuator. The software program enabled us to control the actuator by the computer and to maximize the accuracy of the experiment. From the control unit, displacement of the discs, time and from the load cell, the force information was recorded.

The experimental set-up was designed to give numerical data and visual data; the visual data could be viewed and recorded via the CCD camera (Figure 9). The numerical data was achieved through the use of a load cell, which was mounted on top of the upper plexi-glass disk (Figures 10 and 11). The load cell is connected to an amplifier and multi-meter. The load cell was used to measure the tensile load acting of the fluid; the data was then stored into the computer for further analysis and plotting.

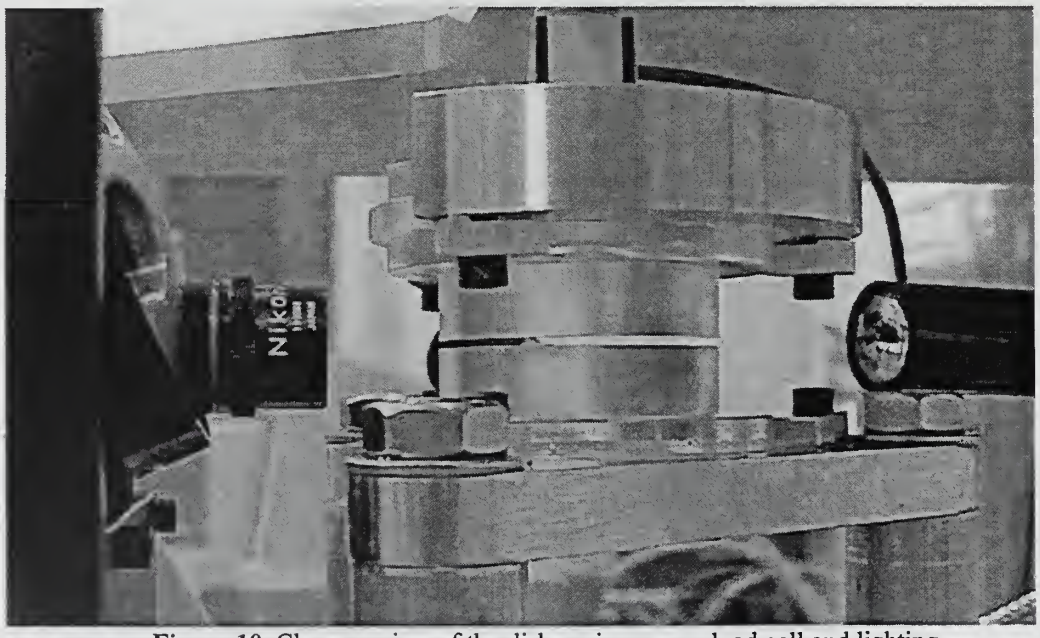

Figure 10. Close-up view of the disks, microscope, load cell and lighting.

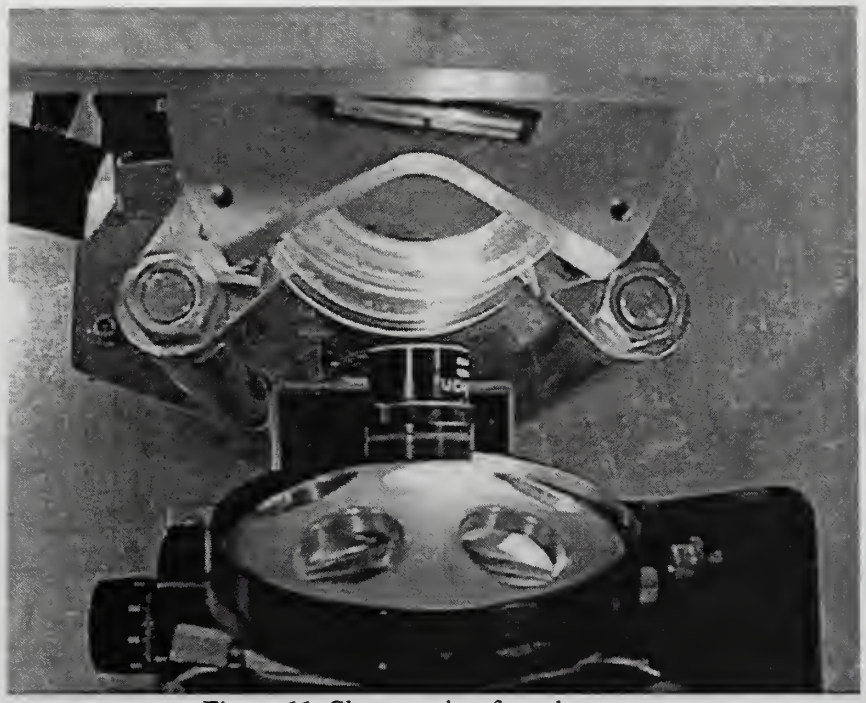

Figure 11. Close-up view from the top.

B. EXPERIMENTAL SET-UP

This section introduces each component of the experimental apparatus and includes a brief description of the component.

1. Silicone Oil

The "Series 200" range of silicone oils from Dow Corning was chosen to be the most appropriate for the purposes of this experimental study. They were commercially able to obtain, that provided a range of medium to high kinematic viscosities (50 – 100,000 cSt) without any appreciable change in surface tension and density. They were easy and safe to work with, and they had advantageous chemical properties. Detailed information about these liquids is presented in Appendix-A.

2. Positioning System

In order for surface tension to dominate viscous forces, the Capillary number (Ca) must be small. For medium to high viscosity silicone oils, a small Capillary number ($10^{-2} - 10^{-6}$) requires velocities to be small as well. Figure 12 presents velocities and Capillary numbers that are associated with different viscosity fluids.

The positioning system control unit was chosen to provide these small velocities. The detailed information about the positioning system is presented in Appendix-B.

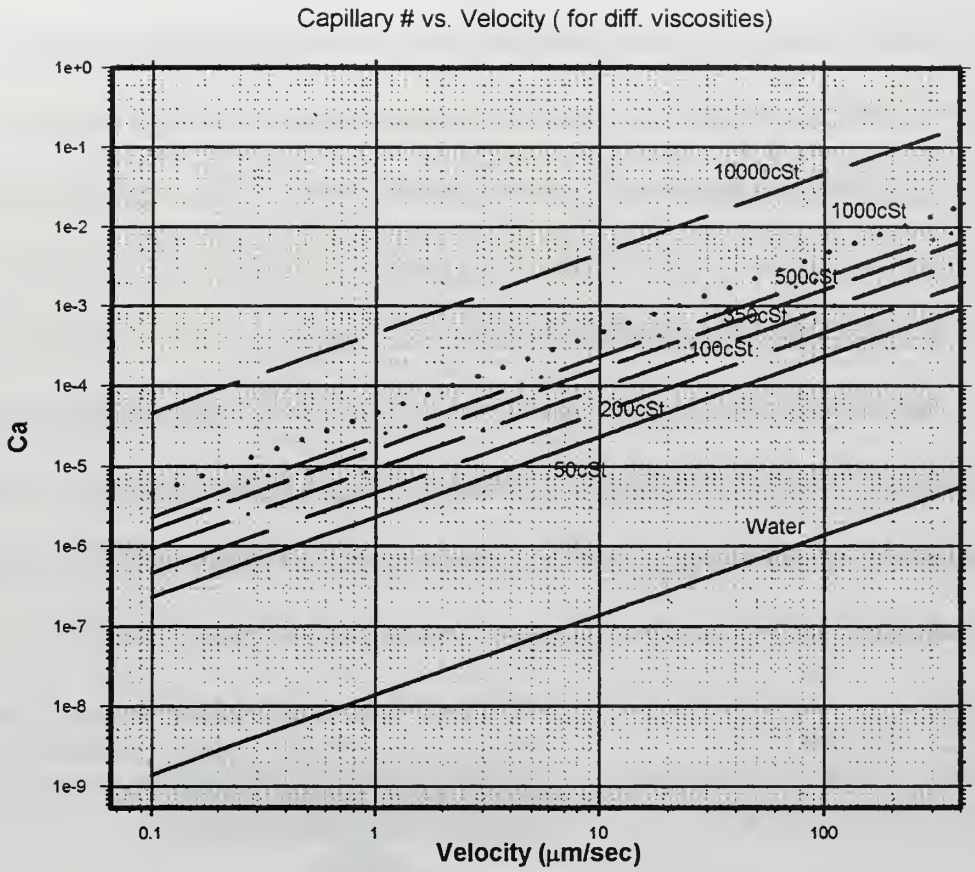

Figure 12. Capillary number vs. Velocity plot.

3. Load Cell

From previous work conducted by (Isik, 1999), the range of forces was already known. Concerns that were critical in determining the type of load cell were, sensitivity, minimum threshold level, resolution level, possible drifting in measurements with time, signal output, size, accuracy, and ability of being used in tension. The specifications and dimensions of the load cells are presented in Appendix-C.

4. Optic Systems

Optical system of the experimental set-up is composed of a microscope that has a lens magnification of 50X and one CCD camera connected to a monitor and/or a VCR. The CCD camera was positioned to achieve a bottom view of the interfacial liquid layer.

C. EXPERIMENTAL PROCEDURE

Experiments have been conducted for 50, 100, 200, 10,000, 60,000, and 100,000 cSt silicone oils. For each silicone oil viscosity a large range of values were used for the initial liquid layer thickness and the separation velocity. A brief list of the variables and ranges are listed below.

LIQUID	: Silicone oil, constant surface tension & density
LIQUID VISCOSITY (υ)	: 50, 100, 200, 10,000, 60,000, 100,000 cSt
LIQUID LAYER THICKNESS (l_o)	: 25, 50, 100 (125), 200 (250), 312.5, 500 μm
SEPARATION VELOCITY (V)	: 1.2 μm/s – 45.5 μm/s

Each experiment was conducted according to the following procedure and schematic diagram of the apparatus is provide in Figure 13:

1) Experimental set-up was turned on to warm-up.
2) Computer program was started and control was transferred to the keyboard.
3) The plexi-glass disks were separated to introduce silicone oil.
4) The silicone oil was spread on the lower disk by an injector.

5) The actuator was moved to position the plexi-glass disks to the desired initial liquid layer thickness. It was made sure that there was no air bubbles in the liquid, and that the liquid had spread completely on both disk surfaces.

6) The velocity, step size and iterations were inputted into the computer program. The computer recorded and displayed step number, time, displacement and force in volts as output. Visual data could be monitored or recorded through the CCD camera.

7) Each run was carried through until separation of the liquid layer occurred.

8) These data have been analyzed by using plots of the force-displacement data force-Capillary number and the visual recorded data.

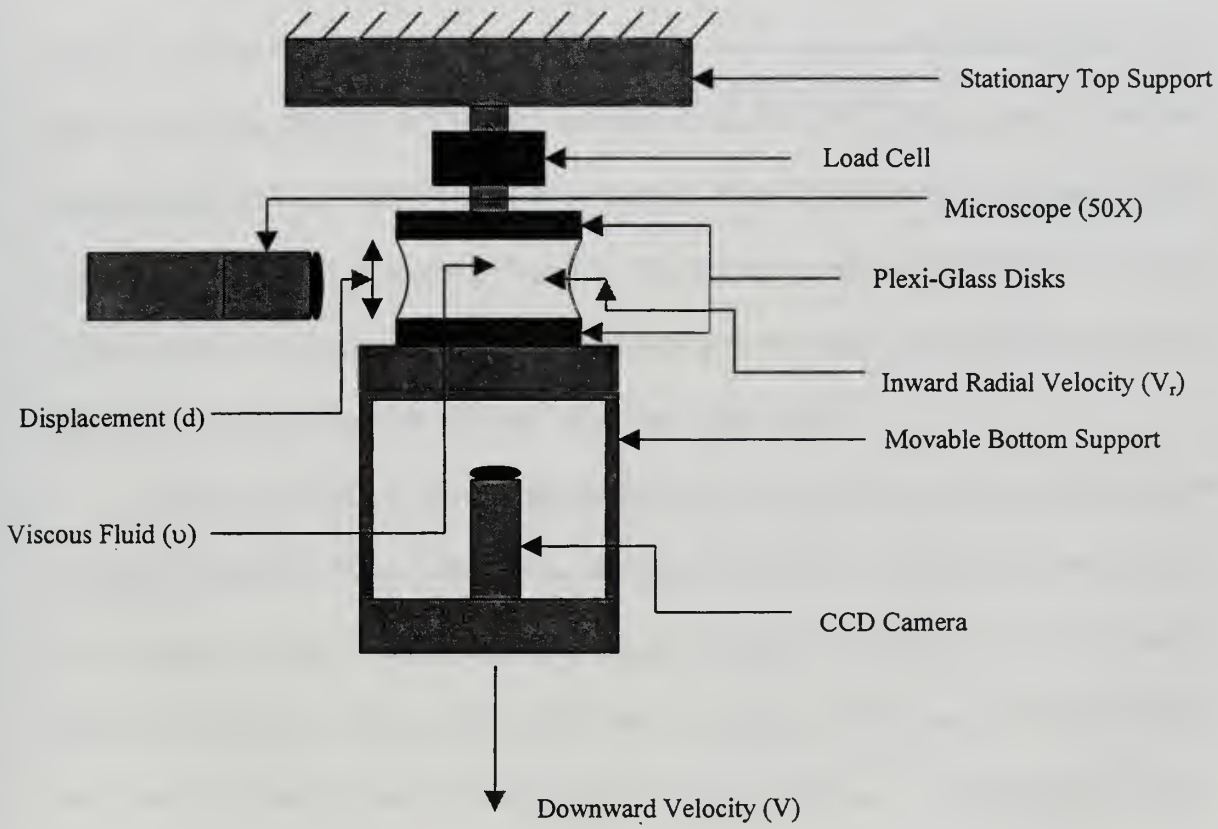

Figure 13. Schematic Diagram of the Experimental Set-up.

THIS PAGE INTENTIONALLY LEFT BLANK

V. RESULTS AND DISCUSSION

A. INTRODUCTION

The experiments were carried out for a wide range of viscosities. A wide range of separation velocities and initial liquid layer thicknesses were also tested. Viscosities ranged from 50 cSt to 100,000 cSt, separation velocities from 1 to 47.5 μm/s, and initial liquid layer thicknesses from 25 to 500 μm were used. Appendix D presents the combinations of these variables.

B. FORCE-DISPLACEMENT PLOTS

The following plots yield the resultant force as the liquid layer is being separated at a constant velocity. The force increases almost linearly to a peak value (F_{max}) and occurs at a plate separation distance (d_{max}) in the liquid layer as explained earlier. The force then drops rapidly and almost instantly to a near zero (steady-state) value and remains there with no further appreciable change. Visually, the sudden decrease in force coincides in the onset of viscous fingering. The medium viscosity fluids (50 – 200 cSt) did not show viscous fingering to the same extent of the high viscosity fluids (10,000 – 100,000), so the decline after the peak value was more subtle.

After reviewing the force-displacement plots, F_{max} and d_{max} were dependent on the initial liquid layer thickness (l_o), the separation velocity (V), the liquid viscosity (υ), and of course surface tension (a special feature of these silicone oils is that the surface tensions is relatively constant throughout the viscosities). Each one of these variables were varied in order to achieve a relationship for F_{max} and d_{max}. The following figures show the dependence of each of the variables for both the medium and high viscosity silicone oils.

1) Fmax, $d_{max} \propto \upsilon$

For a given initial liquid layer thickness (l_o) and separation velocity (V), peak force (F_{max}) and the location of the peak force (d_{max}), increase with increasing liquid viscosity (υ) as shown in Figures 14 and 15. The magnitude of the force differs greatly between the high and medium viscosity silicone oils. This result may be interpreted as the extent of the onset of viscous fingering in the fluid yields greater forces.

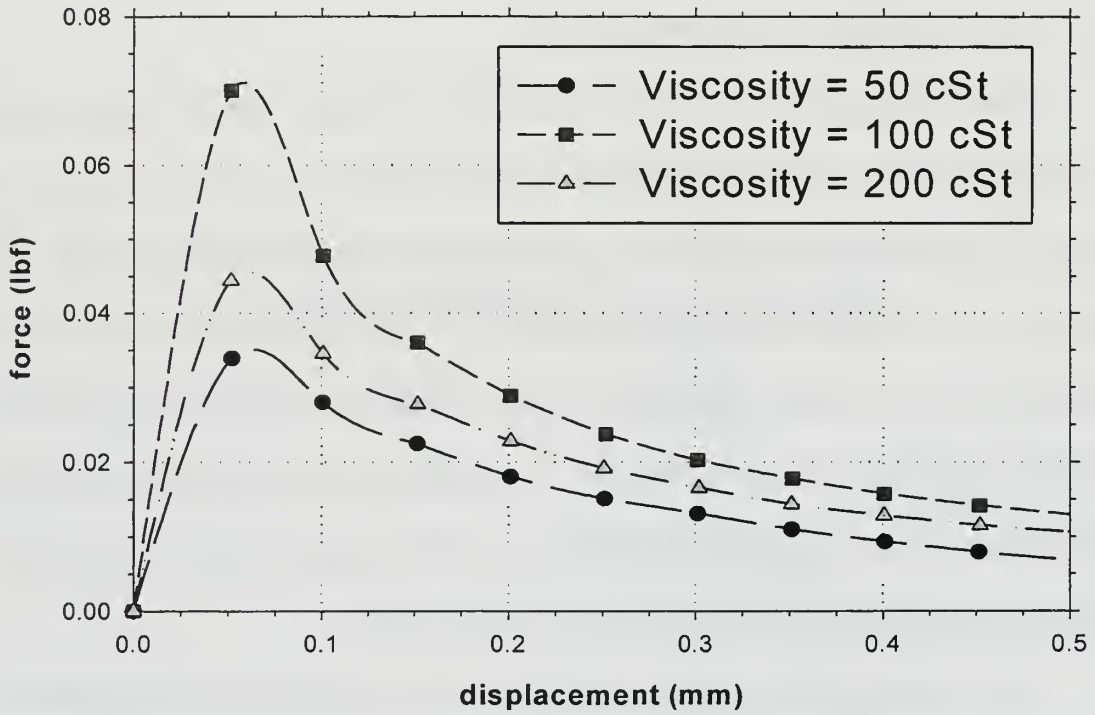

Figure 14. Force-Displacement plot that shows the effect of medium viscosity fluids on F_{max} and d_{max} The Initial Liquid Layer Thickness (l_o) is 50μm, and Separation Velocity (V) is 24μm/s.

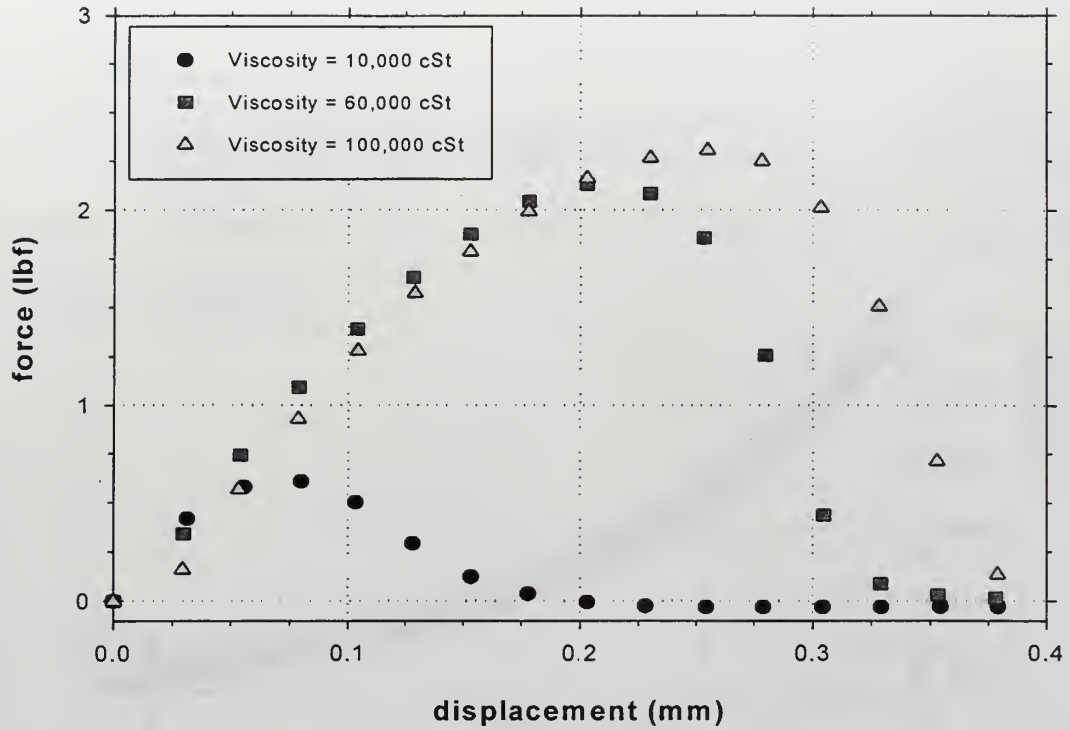

Figure 15. Force-Displacement plot that shows the effect of high viscosity fluids on F_{max} and d_{max} The Initial Liquid Layer Thickness (l_o) is 312μm, and Separation Velocity (V) is 12μm/s.

2) Fmax, $d_{max} \propto V$

For a given liquid viscosity (υ) and initial liquid layer thickness (l_o), peak force (F_{max}) and the location of the peak force (d_{max}), increase with increasing separation velocity (Figures 16 and 17).

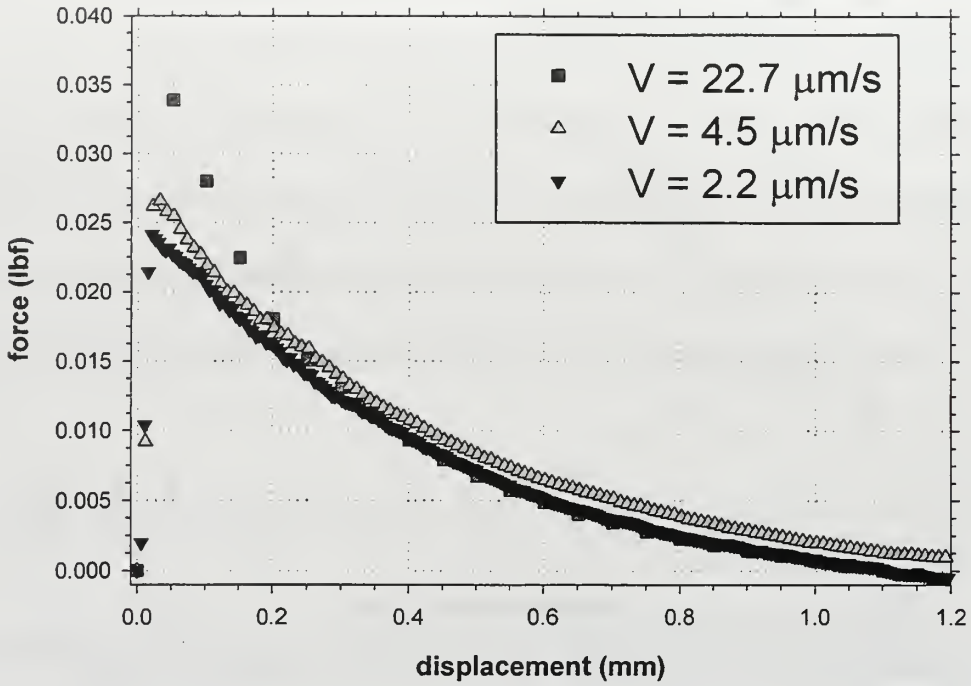

Figure 16. Force-Displacement plot that shows the effect of Separation Velocity on F_{max} and d_{max} The Initial Liquid Layer Thickness (l_o) is 50μm and Viscosity (υ) is 50 cSt.

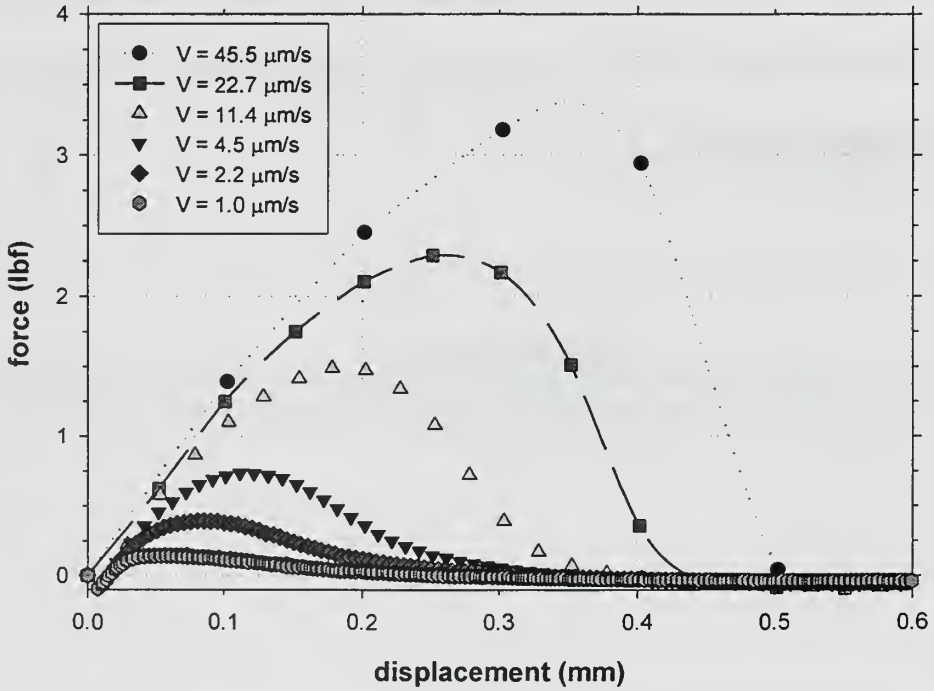

Figure 17. Force-Displacement plot that shows the effect of Separation Velocity on F_{max} and d_{max} The Initial Liquid Layer Thickness (l_o) is 500μm and Viscosity (υ) is 100,000 cSt.

3) Fmax, $d_{max} \propto 1/l_0$

For a given liquid viscosity (υ) and separation velocity (V), peak force (F_{max}) and the location of the peak force (d_{max}), increase with decreasing initial liquid layer thickness (l_o) (Figures 18 and 19).

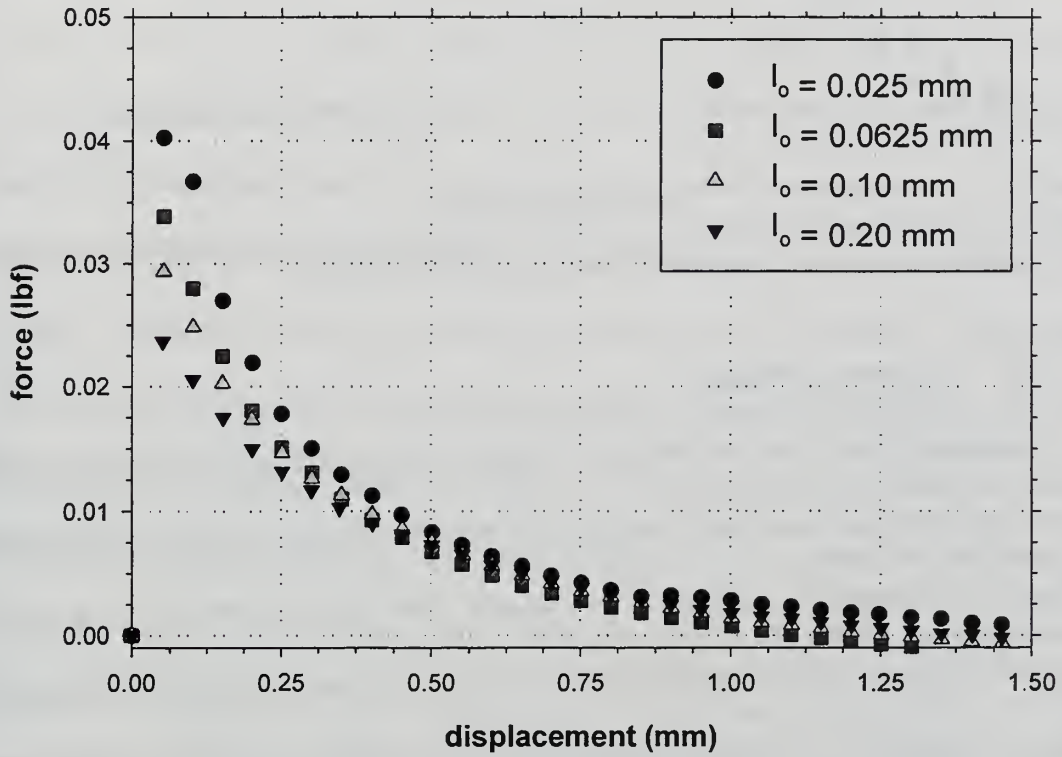

Figure 18. Force-Displacement plot that shows the effect of Initial Liquid Layer Thickness on F_{max} and d_{max} Separation Velocity (V) is 24μm/s and Viscosity (υ) is 50 cSt.

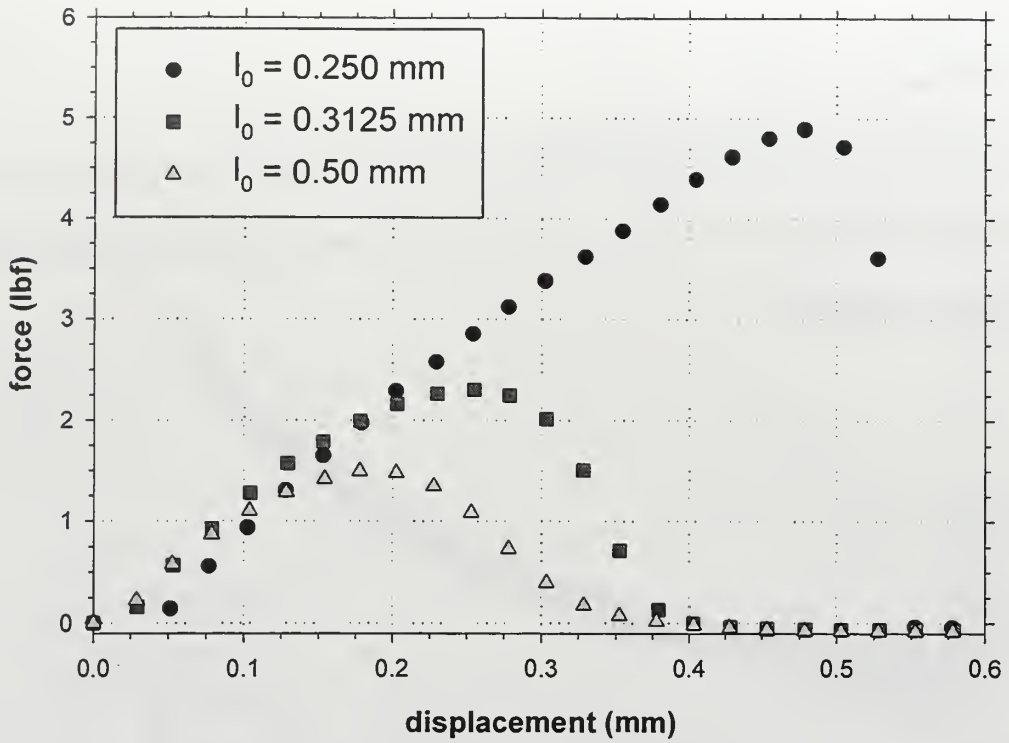

Figure 19. Force-Displacement plot that shows the effect of Initial Liquid Layer Thickness on F_{max} and d_{max} Separation Velocity (V) is 4.5μm/s and Viscosity (υ) is 100,000 cSt.

4) A Physical Model

A model of the force-displacement behavior in the separation mechanics of the layer can be developed based on a creeping flow analysis of the governing Navier-Stokes equations in axisymmetric cylindrical coordinates. The slow motion allows a quasi-steady analysis in which viscous effects are balanced by pressure gradients while inertia effects are negligible. The analysis follows the model problem suggested by Batchelor (1967) or Landau & Lifshitz (1987) and indicates that the separating motion of the two disks creates a negative suction pressure in the liquid layer gap thus resulting a resisting clamping effect opposite to the direction of separation. This resistive force is proportional to liquid viscosity and separation velocity, and inversely proportional to the cube of the liquid layer thickness at any instant, a feature that is qualitatively borne out by the current

study. However a more thorough corroboration between model and experimental data will be considered in future work once more extensive data has been gathered.

C. VISCOUS FINGERING

It was proven that at the instant viscous fingering occurs, the interface in no longer stable. The interface motion is driven by the separation of the two disks. Surface tension serves as a stabilizing entity between the two immiscible fluids. From the discussion in the early chapter on the Saffman-Taylor instability, a critical wavelength was determined at the onset of viscous fingering. At the onset of viscous fingering a number of disturbances develop along the interface called corrugations. At this point the surface tension can no longer stabilize the interface and it is no longer undistorted and circular. The interface is now unstable and continues to grow unstable. If the instability proceeds the interface is no longer balancing the difference in viscosities and pressure differentials to surface tension, the number of corrugations has reached its maximum value and coincides with the maximum resultant force. From the Saffman-Taylor instability analysis of the experimental radial Hele-Shaw the maximum wavelength and number of corrugations were derived. The maximum wavelength is the largest wavelength that gives rise to the viscous fingers that grow the fastest. In order to prevent viscous fingering from occurring and leading to an unstable interface the critical wavelength critical wavelength becomes an important measuring device of instability.

A comparison of various separation velocities and initial liquid layer thickness are considered below. The maximum wavelength and number of corrugations for each run was calculated and compared to the picture at the same instant. Table 1 contains the calculated quantities.

Kinematic Viscosity (cSt)	10000	10000	10000	10000
Surface Tension (N/m)	0.021	0.021	0.021	0.021
Radius (m)	0.0254	0.0254	0.0254	0.0254
Initial Liquid Layer Thickness (m)	0.0002	0.0002	0.0003125	0.0003125
Displacement (mm)	0.029	0.051	0.0328	0.051
Radial Velocity (m/s)	2.80×10^{-4}	3.75×10^{-4}	2.24×10^{-4}	3.0×10^{-4}
Separation Velocity (m/s)	12×10^{-6}	24×10^{-6}	12×10^{-6}	24×10^{-6}
Maximum Wavelength (m)	2.0×10^{-3}	1.90×10^{-3}	3.36×10^{-3}	3.05×10^{-3}
Number of Corrugations	80	84	47	52

Table 1. Experiments conducted for 10,000 cSt Silicone Oil, Calculating Maximum Wavelength and Number of Corrugations.

As initial liquid layer thickness (l_o) decreases, viscous fingering becomes more pronounced, leading to an increase in number of corrugations and a decrease in maximum wavelength. Similarly, separation velocity (V) increases, viscous fingering becomes more pronounced resulting in an increase in the number of corrugations and a decrease in maximum wavelength. Also, separation velocity (V) and the liquid viscosity (υ) also affect the degree of viscous fingering. Higher the separation velocity and liquid viscosity, greater is the extent of viscous fingering.

The following pictures were taken at the maximum growth rate, although the actual number of corrugations can be difficult to identify the same trend as shown above for the maximum wavelength and number of corrugations can be seen.

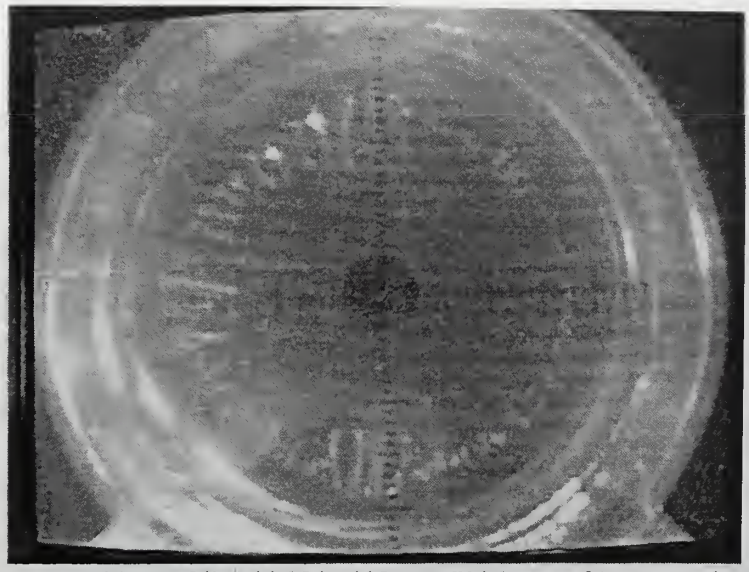

Figure 20. 10,000 cSt Silicone Oil, Initial Liquid Layer Thickness of 200μm and Separation Velocity of 12μm/s (Scale of 1div=1mm), N≈80.

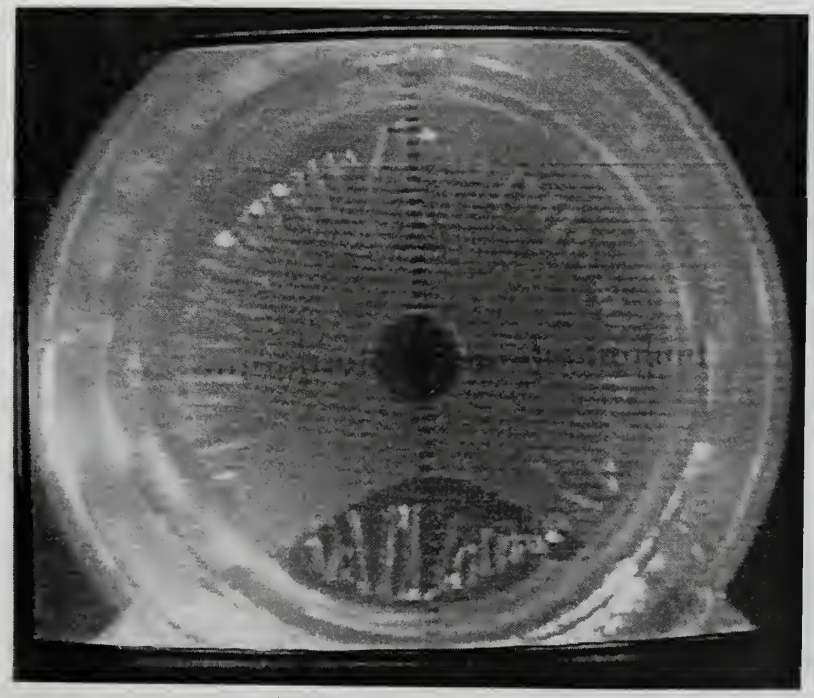

Figure 21. 10,000 cSt Silicone Oil, Initial Liquid Layer Thickness of 200μm and Separation Velocity of 24μm/s (Scale of 1div=1mm), N≈84.

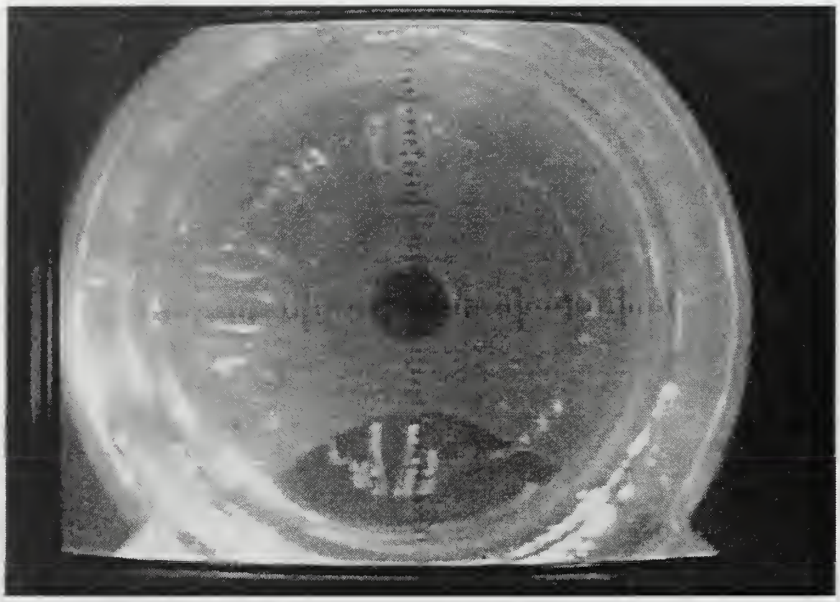

Figure 22. 10,000 cSt Silicone Oil, Initial Liquid Layer Thickness of 312.5μm and Separation Velocity of 12μm/s (Scale of 1div=1mm), N≈47.

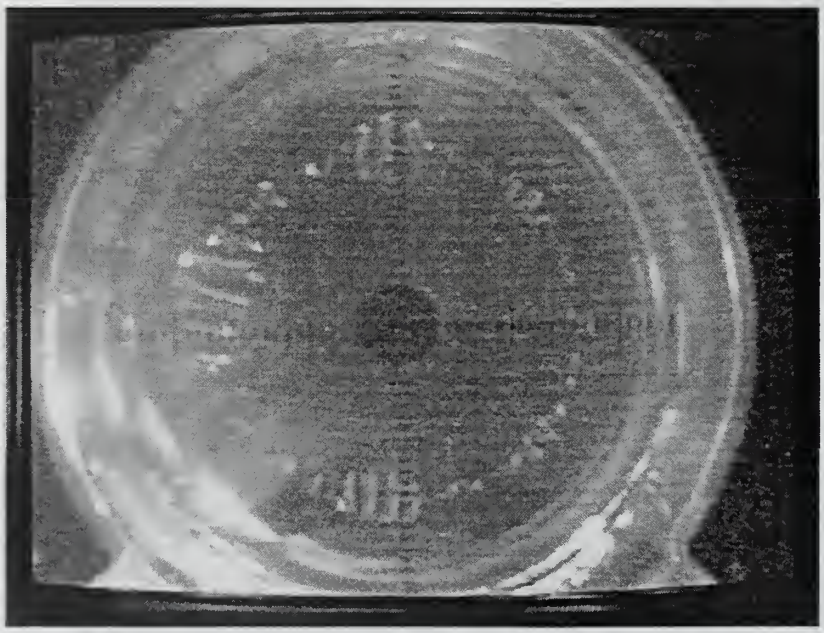

Figure 23. 10,000 cSt Silicone Oil, Initial Liquid Layer Thickness of 312.5μm and Separation Velocity of 24μm/s (Scale of 1div=1mm), N≈52.

VI. CONCLUSIONS AND RECOMMENDATIONS

Well-defined trends in the force-displacement behavior of thin liquid layers were identified from the analysis of the recorded quantitative and qualitative data in this experimental study. A wide range of viscosities were examined and all force-displacement curves have lead to the observation of the presence of a peak force (F_{max}) whose location and value depend on initial liquid layer thickness, separation velocity, liquid viscosity, and surface tension.

The presence of the peak force is more pronounced and its occurrence coincides with the onset of the viscous fingering mechanism. The approach to the peak force (F_{max}) on the force-displacement plot, is accompanied by an instantaneous and sudden decrease in force which is followed by a near zero (steady-state) value with no further appreciable change. The linear stability analysis allows a fairly accurate prediction of the onset of the viscous fingering behavior and correlates well with the experimental data.

Further research on this subject is highly desirable to widen the parametric study to other viscosity ranges and surface tension. A more accurate characterization of the interface velocity is crucial to further the understanding of the onset of viscous fingering and its dependence on the Capillary number. A review and refinement of the analytical model may also be conducted and balanced with the necessary boundary conditions, which could lead to corroboration with the different observed regimes.

In addition, a more advanced and integrated testing apparatus with better measurement abilities of the interface velocity, layer thickness, actuator motion and interface flatness and parallelism is required. It would also be desirable to increase the data acquisition rate to at least the milli-second level in order obtain more accurate force-

displacement information. The use of an optical grade glass, instead of plexi-glass, for the disk would be advantageous to ensure smooth, flat and parallel, and hard (scratch-resistant) surfaces.

APPENDIX – A

SILICONE OIL

Medium Viscosity Silicone Fluids:

200® Fluid, 50 cSt
200® Fluid, 100 cSt
200® Fluid, 200 cSt

High Viscosity Silicone Fluids:

200® Fluid, 10,000 cSt
200® Fluid, 60,000 cSt
200® Fluid, 100,000 cSt

Description:

200® Fluids from Dow Corning, 50 – 1,000 centistokes (cSt) are medium, and 10,000 – 100,000 centistokes (cSt), are high viscosity polydimethylsiloxane polymers manufactured to yield linear polymers with average kinematic viscosities ranging from 50 – 1000 cSt and 10,000 – 100,000 cSt.

Composition:

Linear polydimethylsiloxane polymers characteristically have the following typical chemical composition:

$$(CH_3)_3SiO[SiO(CH_3)_2]_nSi(CH_3)_3$$

Commercial bulk polymerized dimethl silicone fluids, such as *200*® Fluids typically contain trace amounts of process impurities.

Benefits:

200® Fluids, 50 – 100,000 cSt, have the following product characteristics;

- ► Clear
- ► Nongreasy
- ► Nonocclusive
- ► Non-stinging on skin

200® Fluids, 50 – 100,000 cSt, when compared with other materials that may be substituted in a given application, may offer one or more of these comparative characteristics:

- High compressibility
- High oxidation resistance
- High temperature serviceability
- High spreadibility
- Low fire hazard
- Low reactivity
- Low temperature serviceability
- Good heat stability
- Good leveling and easy rubout
- High damping action
- High shear-ability without breakdown
- High compatibility
- High water repellency
- Low odor
- Low surface energy
- Low vapor pressure
- Soft feel and lubricity on skin

APPENDIX – B

POSITIONING SYSTEM

Model 855 Programmable Controller System (Newport Corporation)

The Model 855 Programmable Controller is a microprocessor-based system that allows simultaneous direct or programmable control of up to four Newport linear actuators or rotary stages. It is simple but powerful vocabulary of mnemonic commands allows straightforward programming and control via the handheld 855K Keypad/Display.

The 855C Controller:

The 855C Programmable Controller is the nucleus of a system that automatically controls up to four Newport precision positioners and stages. Its large, easy-to-learn instruction set and standard RS-232C and IEEE-488 interface ports allow it to work closely with external computers and other data devices. Its programmability provides stand-alone automatic control of actuator motion, yet no knowledge of programming techniques is required. It also supports the optional 855K handheld Keypad/Display for convenient data entry, control and program editing.

Specifications:

Actuator Control:	Provides ±15 VDC, 1.5 Amp power and ±10V velocity control signals for up to 4 Newport linear positioning devices. Receives and decodes dual output, 90° phase, +12.5, -0.5 V encoder pulses and limit signals.
CPU:	8 bit 6809 high-performance micro-processor
RAM:	4 Kbytes
PROM:	24 Kbytes
EPROM:	2 Kbytes
I/O:	RS-232C Serial Port/IEEE-488 Parallel Port
Power:	110-220 VAC, 50/60 Hz and 850 mA with all actuators fully loaded.
Dimensions:	5.25" high X 17" wide X 12" deep

The 855K Keyboard/Display:

The 855K can be used to completely control and program the 855C. It is handy for manual control of actuator position and for the reviewing and editing 855C programs. Its backlit alphanumeric liquid-crystal display shows position information for the four drivers, programming instructions for the 855C, and messages from the 855C. The 855K's keypad has 35 durable, tactile-response membrane keys for command and data entry. The 855K connects to the 855C via a coiled cable.

The Linear Actuators:

The 855C is compatible with Newport's 850 Series Linear Actuators. Each of these devices use DC motor drives with integral optical encoders for smooth operation and high resolution. The 855C fully supports their resolution and range. Only one actuator is used for this experimental study.

APPENDIX – C

LOAD CELL

Since the viscosities of the fluids differed greatly from 50 cSt to 100,000 cSt, there was a need to use two different load cells for the experiments. For higher viscosities an MLP-100 (100 lb maximum load) and for the lower viscosities the MDP-2.5 (2.5 lb maximum load) were used. The specifications are listed below for each load cell.

MLP-100 Specifications:

MINI LOW PROFILE LOAD CELL
UNIVERSAL / TENSION OR COMPRESSION

The model MLP Series load cells were designed with economy as first priority. The MLP Series are anodized aluminum with a unique low profile design, which provides excellent stability for in line application for tension and/or compression.

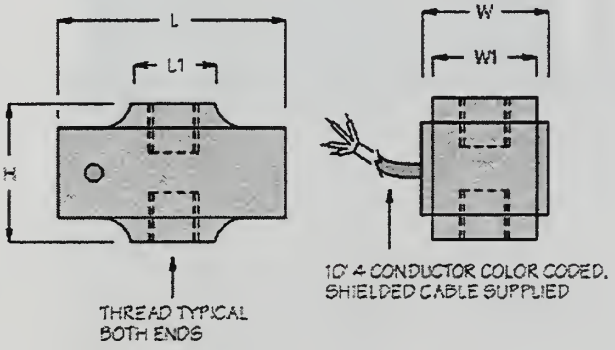

SPECIFICATIONS

Rated Output (R.O.):	2 mV/V nominal
Nonlinearity:	0.05% of R.O.
Hysteresis:	0.05% of R.O.
Nonrepeatability:	0.05% of R.O.
Zero Balance:	1.0% of R.O.
Compensated Temp. Range:	60° to 160°F
Safe Temp. Range:	-65° to 200°F
Temp. Effect on Output:	0.005% of Load/°F
Temp. Effect on Zero:	0.005% of R.O./°F
Terminal Resistance:	350 ohms nominal
Excitation Voltage:	10 VDC
Safe Overload:	150% of R.O.
Weight:	1 oz. all ranges

DIMENSIONS (INCHES)

MODEL	CAPACITY LBS.	L	L1	W	W1	H	THREAD	THREAD DEPTH
MLP-10	10	1.504	.600	.54	.375	.75	10-32	.200
MLP-25	25	1.521	.600	.66	.500	.75	1/4-28	.230
MLP-50	50	1.584	.625	.66	.500	.75	1/4-28	.230
MLP-75	75	1.640	.650	.66	.500	.75	1/4-28	.230
MLP-100	100	1.684	.660	.66	.500	.75	1/4-28	.230
MLP-150	150	1.642	.575	.93	.750	1.00	3/8-24	.375
MLP-200	200	1.688	.580	.93	.750	1.00	3/8-24	.375
MLP-300	300	1.748	.600	.93	.750	1.00	3/8-24	.375
MLP-500	500	1.658	.580	.93	.750	1.00	3/8-24	.375
MLP-750	750	1.734	.585	.93	.750	1.00	3/8-24	.375
MLP-1K	1,000	1.784	.615	.93	.750	1.00	3/8-24	.375

MDB-2.5 Specifications:

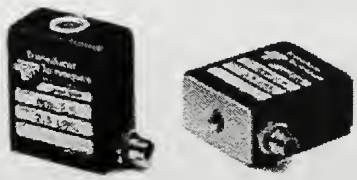

ULTRA PRECISION MINI LOAD CELL
UNIVERSAL / TENSION OR COMPRESSION

The MDB Series was designed to help fill the growing need for a greater selection of high accuracy load cells for use in space limited applications. The anodized aluminum MDB's are compliant tension and compression, therefore, a good choice for in line through zero applications, as well as single direction tension or compression.

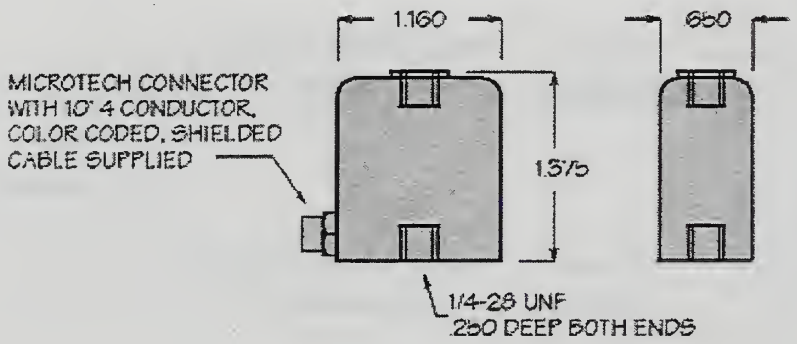

SPECIFICATIONS

Rated Output (R.O.):	2 mV/V nominal
Nonlinearity:	0.05% of R.O.
Hysteresis:	0.05% of R.O.
Nonrepeatability:	0.05% of R.O.
Zero Balance:	1.0% of R.O.
Compensated Temp. Range:	60° to 160°F
Safe Temp. Range:	-65° to 200°F
Temp. Effect on Output:	0.005% of Load/°F
Temp. Effect on Zero:	0.005% of R.O./°F
Terminal Resistance:	350 ohms nominal
Excitation Voltage:	10 VDC
Safe Overload:	150% of R.O.
Weight:	1 oz. all ranges

THIS PAGE INTENTIONALLY LEFT BLANK

APPENDIX – D

EXPERIMENTAL DATA

50, 100, 200 cSt Silicone Oil	**Initial Liquid Layer Thickness (l_o)** 25μm	**Velocity (μm/s)**	48
			24
			12
			4.5
			2.4
			1.2
	Initial Liquid Layer Thickness (l_o) 50μm	**Velocity (μm/s)**	48
			24
			12
			4.5
			2.4
			1.2
	Initial Liquid Layer Thickness (l_o) 100μm	**Velocity (μm/s)**	48
			24
			12
			4.5
			2.4
			1.2
	Initial Liquid Layer Thickness (l_o) 200μm	**Velocity (μm/s)**	48
			24
			12
			4.5
			2.4
			1.2
	Initial Liquid Layer Thickness (l_o) 312μm	**Velocity (μm/s)**	48
			24
			12
			4.5
			2.4
			1.2
	Initial Liquid Layer Thickness (l_o) 500μm	**Velocity (μm/s)**	48
			24
			12
			4.5
			2.4
			1.2

Table 1. 50, 100, 200 cSt silicone oils and their varying parameters.

10,000, 60,000, 100,000 cSt Silicone Oil	**Initial Liquid Layer Thickness (l_o)** 125μm	**Velocity (μm/s)**	48
			24
			12
			4.5
			2.4
			1.2
	Initial Liquid Layer Thickness (l_o) 250μm	**Velocity (μm/s)**	48
			24
			12
			4.5
			2.4
			1.2
	Initial Liquid Layer Thickness (l_o) 312μm	**Velocity (μm/s)**	48
			24
			12
			4.5
			2.4
			1.2
	Initial Liquid Layer Thickness (l_o) 500μm	**Velocity (μm/s)**	48
			24
			12
			4.5
			2.4
			1.2

Table 1. 10,000, 60,000, 100,000 cSt silicone oils and their varying parameters.

LIST OF REFERENCES

Batchelor, G. K., *An Introduction to Fluid Dynamics*, Cambridge University Press, 1967.

Landau, L. D. and Lifshitz, E. M., *Fluid Mechanics,* Pergamon Press, 1987.

Faber, T. E., *Fluid Dynamics for Physicists*, Cambridge University Press, 1997.

Maxworthy, T., *Experimental Study of Interface Instability in a Hele-Shaw Cell*, The American Physical Society (1989), vol. 39, 11.

Paterson, Lincoln, *Radial Fingering in a Hele-Shaw Cell*, Journal of Fluid Mechanics (1981), vol. 113, 513-529.

Probstein, Ronald F., *Physicochemical Hydrodynamics*, Butterworths, 1989.

Saffman, P. G., *Selection Mechanisms and Stability of Fingers and Bubbles in Hele-Shaw Cells*, IMA Journal of Applied Mathematics (1991), 46, 137-145.

Saffman, P. G. and Taylor, G. I., *The Penetration of a Fluid into a Porous Medium or Hele-Shaw Cell Containing a More Viscous Liquid*, Proc. R. Soc. Lond., 1958.

Schlichting, Herman, *Boundary Layer Theory*, McGraw-Hill, Inc., 1979.

Isik, Sefa, *A Preliminary Experimental Study of the Behavior of Liquids under Tension*, Master's Thesis, Naval Postgraduate School, Monterey, California, June 1999.

Sherman, Frederick S., *Viscous Flow*, McGraw-Hill, Inc., 1990.

Taylor, G. I., *Cavity Flows of Viscous Liquids in Narrow Spaces*, Proc. 2nd Symp., Naval Hydrodynamics, 1958.

Taylor, G. I. and Saffman P. G., *A Note on the Motion of Bubbles in a Hele-Shaw Cell and Porous Medium*, Q. J. Mech. Appl. Math., 1958.

White, F. M., *Fluid Mechanics*, McGraw-Hill, Inc.,3rd Ed., 1994.

THIS PAGE INTENTIONALLY LEFT BLANK

INITIAL DISTRIBUTION LIST

No. Copies

1. Defense Technical Information Center.....2
   8725 John J. Kingman Rd., STE 0944
   Ft. Belvoir, VA 22060-6218

2. Dudley Knox Library.....2
   Naval Postgraduate School
   411 Dyer Rd.
   Monterey, CA 93943-5101

3. Chairman, Code ME.....1
   Department of Mechanical Engineering
   Naval Postgraduate School
   Monterey, CA 93943-5000

4. Professor Ashok Gopinath, Code ME/Gk.....2
   Department of Mechanical Engineering
   Naval Postgraduate School
   Monterey, CA 93943-5000

5. Naval/Mechanical Engineering Curricular Office, Code 34.....1
   Naval Postgraduate School
   Monterey, CA 93943-5000

6. Commanding Officer (Code C35).....2
   Naval School, Civil Engineer Corps Officers
   Naval Construction Battalion Center
   Port Hueneme, CA 93043

7. Christopher H. Rehkop.....3
   6104 Summit Pointe Road
   Harrisburg, PA 17111